

# ES-GNN: Generalizing Graph Neural Networks Beyond Homophily with Edge Splitting

Jingwei Guo

Jingwei.Guo@liverpool.ac.uk  
University of Liverpool  
Liverpool, UK

Xinping Yi

Xinping.Yi@liverpool.ac.uk  
University of Liverpool  
Liverpool, UK

Kaizhu Huang\*

Kaizhu.Huang@dukekunshan.edu.cn  
Duke Kunshan University  
Suzhou, China

Rui Zhang

Rui.Zhang02@xjtlu.edu.cn  
Xi'an Jiaotong-Liverpool University  
Suzhou, China

## ABSTRACT

Graph Neural Networks (GNNs) have achieved enormous success in tackling analytical problems on graph data. Most GNNs interpret nearly all the node connections as inductive bias with feature smoothness, and implicitly assume strong homophily on the observed graph. However, real-world networks are not always homophilic, but sometimes exhibit heterophilic patterns where adjacent nodes share dissimilar attributes and distinct labels. Therefore, GNNs smoothing the node proximity holistically may aggregate inconsistent information arising from both task-relevant and irrelevant connections. In this paper, we propose a novel edge splitting GNN (ES-GNN) framework, which generalizes GNNs beyond homophily by jointly partitioning network topology and disentangling node features. Specifically, the proposed framework employs an interpretable operation to adaptively split the set of edges of the original graph into two exclusive sets indicating respectively the task-relevant and irrelevant relations among nodes. The node features are then aggregated separately on these two partial edge sets to produce disentangled representations, based on which a more accurate edge splitting can be attained later. Theoretically, we show that our ES-GNN can be regarded as a solution to a graph denoising problem with a disentangled smoothness assumption, which further illustrates our motivations and interprets the improved generalization. Extensive experiments over 8 benchmark and 1 synthetic datasets demonstrate that ES-GNN not only outperforms the state-of-the-arts (including 8 GNN baselines), but also can be more robust to adversarial graphs and alleviate the over-smoothing problem.

## 1 INTRODUCTION

As a ubiquitous data structure, graph can symbolize complex relationships between entities in different domains. For example, knowledge graphs describe the inter-connections between real-world events, and social networks store the online interactions between users. With the flourishing of deep learning models on graph-structured data, graph neural networks (GNNs) emerge as one of the most powerful techniques in recent years. Owing to their remarkable performance, GNNs have been widely adopted in multiple graph-based learning tasks, such as link prediction, node classification, and recommendation [6, 12, 35].

Modern GNNs are mainly built upon a message passing mechanism [9], where nodes' representations are learned by iteratively aggregating their transformed neighbors. From the graph signal denoising viewpoint, this mechanism could be seen as a low-pass filter [18, 31, 38] that smooths the signals between adjacent nodes. Notably, it works well on homophilic (assortative) graphs, from which the proximity information of nodes can be utilized to predict their labels [21]. However, real-world networks are typically abstracted from complex systems, and sometimes display heterophilic (disassortative) properties whereby the opposite objects are attracted to each other [19]. For instance, different types of amino acids are mostly interacted in many protein structures [37], and most people prefer to link with others of the opposite gender in heterosexual dating networks. Recent studies [5, 7, 27, 30, 36, 37] have shown that the conventional neighborhood aggregation strategy may not only cause the over-smoothing problem [22] but also severely hinder the generalization performance of GNNs beyond homophily.

One reason why current GNNs perform poorly on heterophilic graphs, could be the mismatch between the labeling rules of nodes and their linking mechanism. The former is the target that GNNs are expected to learn for classification tasks, while the latter specifies how messages pass among nodes for attaining this goal. In homophilic scenarios, both of them are similar in the sense that most nodes are linked because of their commonality which therefore leads to identical labels. In heterophilic scenarios, however, the motivation underlying why two nodes get connected may be ambiguous to the classification task. Let us take the social network within a university as an example, where students from different clubs can be linked usually because of taking the same classes but not sharing the same hobbies. Namely, the node neighborhood under heterophily is typically entangled with the task-relevant and irrelevant (or even misleading) information. The existing methods usually fail to distinguish these two types of information within nodes' proximity, and the learned representations are consequently prone to preserve erroneous information, leading to non-robustness and sub-optimal results.

Once the issue of GNNs' learning beyond homophily is identified, a natural question arises: *Can we design a new type of GNNs that is adaptive to both homophilic and heterophilic scenarios?* Well formed designs should be able to recognize the node connections irrelevant to learning tasks, and substantially extract the most correlated information for prediction. However, real-world networks

\*Corresponding Author

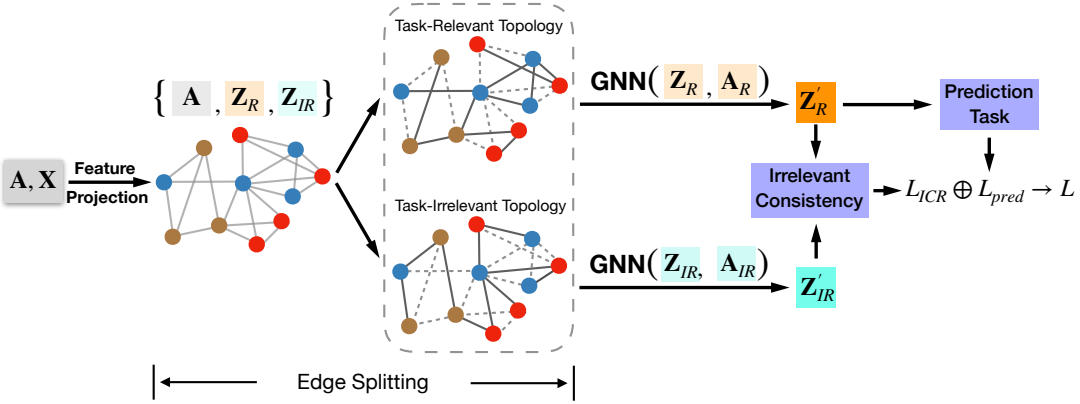


Figure 1: Illustration of our ES-GNN framework with one hidden layer, where  $A$  and  $X$  denote the adjacency matrix and feature matrix of nodes, respectively. First,  $X$  is projected onto different latent subspaces in different channels  $R$  and  $IR$ . An edge splitting is then performed to divide the original graph edges into two exclusive sets, on which information is aggregated individually and separately to produce disentangled representations. The task-relevant representation  $Z'_R$  is reasonably granted for prediction. On the other hand, an Irrelevant Consistency Regularization (ICR) is further developed to regulate the task-irrelevant representations  $Z'_IR$  for capturing the least correlated information to learning tasks.

usually exhibit diverse connecting patterns wherein the assortative parts of the graph are typically mixed with the disassortative. Conventional attention mechanism focuses on measuring the similarity between pairwise node features [13, 29], and cannot well assess the correlation between node connections and the downstream target.

In this paper, we propose ES-GNN, an end-to-end graph learning framework that generalizes GNNs on graphs with either homophily or heterophily. Without loss of generality, we make an assumption that two nodes get connected mainly because they share some similar features, which are however unnecessarily just relevant to the learning task. Namely, they may be linked due to similar features, either relevant or irrelevant to the task. This implicitly divides the original graph edges into two exclusive sets, each of which represents a latent relation between nodes. Thanks to the proximity smoothness, aggregating node features individually on each edge set should disentangle the task-relevant and irrelevant features. Meanwhile, these disentangled representations potentially reflect node similarity in two aspects (task-relevant and irrelevant). As such, they can be better utilized to split the original graph edges more precisely. Motivated by this, the proposed framework integrates GNNs with an interpretable edge splitting (ES), to jointly partition network topology and disentangle node features.

Technically, we design a residual scoring mechanism, executed within each ES-layer, to distinguish the task-relevant and irrelevant connections among nodes. The node features are then allowed to propagate separately along these connections to produce disentangled representations, based on which graph edges can be classified more accurately in the next ES-layer. Finally, the task-relevant representation is granted for prediction. Meanwhile, we develop an Irrelevant Consistency Regularization (ICR) to regulate the task-irrelevant representations for capturing the least correlated information to the learning task at hand. To interpret our new algorithm theoretically, generalizing the smoothness assumption, we

also conduct some analysis on ES-GNN and establish its connection with a graph signal denoising problem.

To summarize, the main contributions of this work are three-fold:

- We propose a novel framework called ES-GNN for node classification tasks, which enables GNNs to go beyond the strong homophily assumption on graphs.
- We theoretically prove that our ES-GNN is equivalent to solving a graph denoising problem with a disentangled smoothness assumption, which interprets the improved generalization power on different types of networks.
- Extensive evaluations on 8 benchmark and 1 synthetic datasets show that ES-GNN consistently outperforms the state-of-the-art GNNs on graphs with various homophily levels, and give the largest error reduction of 17.4%. More importantly, our ES-GNN enjoys a remarkable robustness against adversarial graphs and is able to alleviate the over-smoothing problem.

## 2 RELATED WORK

GNNs have achieved outstanding performance in many tasks [3, 11, 34] by fusing network topology and node content with a message passing framework [9]. In GNNs, it propagates node features across edges followed by a neighborhood aggregation. The core idea is to utilize the proximity information of nodes for building their representations, based on which great effort has been made in developing different variants [15, 16, 29, 31–33], and understanding the nature of GNNs [4, 8, 18, 38]. From the viewpoint of signal processing, GNNs essentially behave as a low pass filter that smooths information within nodes’ surroundings [20, 21, 31]. In line with this view, Zhu et al. [38] and Ma et al. [18] show that a number of GNN models can be seen as different optimization solvers to a graph signal denoising problem with the smoothness assumption upon pairwise nodes. All these results indicate GNNs implicitly assume

strong homophily on the observed graphs while largely overlooking the important setting of heterophily, where node features and labels vary unsmoothly. Furthermore, it is well established that the conventional aggregation strategy leads to the over-smoothing problem [22].

To alleviate this issue, several works are designed to leverage the long-range information beyond nodes' proximity. Geom-GCN [23] extends the standard message passing with geometric aggregation in a structural latent space. H2GCN [37] directly models the higher order neighborhoods for capturing the homophily-dominant information. WRGAT [4] transforms the input graph into a multi-relational graph, for modeling structural information and enhancing the assortativity level. GEN [30] estimates a suitable graph for GNNs' learning with multi-order neighborhood information and Bayesian inference as guide. Another line of work emphasizes the proper utilization of node neighbors. The most common works employ attention mechanism [10, 29], however, they are still imposing smoothness within nodes' neighborhood albeit on the important members only. FAGCN [5] adaptively extracts and integrates both similarities and distinctions between node pairs. Similarly, GPR-GNN [7] introduces a polynomial graph filter, which associates different hop neighbors with learnable weights in different signs, and models both low- and high-frequency information. However, none of them analyzes the motivations why two nodes get connected, nor do they associate them with the downstream learning tasks, which is considered as the key to generalize GNNs on different types of networks in this paper.

### 3 PRELIMINARIES

Let  $\mathcal{G} = (\mathcal{V}, \mathcal{E})$  represents an undirected graph with adjacency matrix  $\mathbf{A} \in \mathbb{R}^{|\mathcal{V}| \times |\mathcal{V}|}$ , where  $\mathcal{V}$  denotes the node set,  $\mathcal{E}$  denotes the edge set, and  $|\mathcal{V}|$  is the number of nodes. We define  $(v_i, v_j) \in \mathcal{E}$ ,  $v_i, v_j \in \mathcal{V}$ ,  $i \neq j$  if  $v_i$  and  $v_j$  are connected, and  $\mathcal{N}_i = \{v_j | (v_i, v_j) \in \mathcal{E}\}$  as the neighborhood of node  $v_i$ . The nodes are associated with a feature matrix  $\mathbf{X} \in \mathbb{R}^{|\mathcal{V}| \times f}$  where  $f$  is the number of raw features, and we use  $\mathbf{X}_{[i, :]} \in \mathbb{R}^f$  to denote the  $i^{th}$  row of  $\mathbf{X}$ . We consider the standard node classification task on undirected graphs, where each node  $v_i$  has a ground truth vector  $\mathbf{y}_i \in \mathbb{R}^C$  in one-hot encoding where  $\mathbf{y}_i(c_i) = 1$  and  $c_i$  is the assigned label out of  $C \leq |\mathcal{V}|$  classes.

### 4 FRAMEWORK: ES-GNN

In this section, we propose an end-to-end graph learning framework, ES-GNN, generalizing Graph Neural Networks (GNNs) to arbitrary graph-structured data with either homophilic or heterophilic properties. An overview of ES-GNN is given in Figure 1. The central idea is to integrate GNNs with an interpretable edge splitting (ES) layer that adaptively partitions the network topology as guide to disentangle the task-relevant and irrelevant node features.

#### 4.1 Edge Splitting Layer

The goal of this layer is to infer the latent relation underlying adjacent nodes, and distinguish between graph edges which could be relevant or irrelevant to the node classification task. Given a simple graph with an adjacency matrix  $\mathbf{A}$  and node feature matrix  $\mathbf{X}$ , an ES-layer splits the original graph edges into two exclusive

sets, which induces two partial network topologies with symmetric matrices  $\mathbf{A}_R, \mathbf{A}_{IR} \in \mathbb{R}^{|\mathcal{V}| \times |\mathcal{V}|}$  storing respectively the splitting coefficients  $a_{R(i,j)}, a_{IR(i,j)} \in (0, 1)$ . We would expect  $\mathbf{A}_R$  and  $\mathbf{A}_{IR}$  to be exclusive, s.t.  $\mathbf{A}_R + \mathbf{A}_{IR} = \mathbf{A}$ , and distinct, so as to capture the task-relevant and irrelevant relations between nodes in a latent space, separately.

However, measuring the correlation between each node connection and the classification task is of great challenge as the assortativity of real-world networks is usually agnostic. Simply applying the attention mechanism as in Graph Attention Network [29] does not necessarily ensure the expected *exclusiveness* and *distinction*. To this end, we design a residual scoring mechanism based on one plausible hypothesis defined below.

**Hypothesis 1.** Two nodes get connected in a graph mainly due to their similarity in some features, which could be *either relevant or irrelevant to the learning task*.

This hypothesis is assumed without losing generality to both homophilic and heterophilic graphs. For a homophilic scenario, e.g., in citation networks, scientific papers tend to cite or be cited by others from the same area, and both of them usually possess the common keywords uniquely appearing in their topics. For a heterophilic scenario, students having different interests are likely be connected because of the same classes they take or the same dormitory they live in, but neither has direct relation to the clubs they have joined. This inspires us to classify graph edges by measuring the similarity between adjacent nodes in two different aspects, i.e., a graph edge is more relevant to the classification task if the connected nodes are more similar in their task-relevant features, or otherwise.

An ES-layer consists of two channels to respectively extract the task-relevant and irrelevant information from nodes. As only the raw feature matrix  $\mathbf{X}$  is provided in the beginning, we will project them into two different subspaces in the first ES-layer:

$$\mathbf{Z}_s^{(0)} = \sigma(\mathbf{W}_s^T \mathbf{X} + \mathbf{b}_s), \quad (1)$$

where  $\mathbf{W}_s \in \mathbb{R}^{f \times \frac{d}{2}}$  and  $\mathbf{b}_s \in \mathbb{R}^{\frac{d}{2}}$  are the learnable parameters in channel  $s \in \{R, IR\}$ , and  $\sigma$  is a nonlinear activation function.

Instead of directly introducing metrics between adjacent nodes to learn the splitting coefficients  $a_{R(i,j)}$  and  $a_{IR(i,j)}$  independently, we propose an integration by predicting their residual scores  $\alpha_{i,j} \in (-1, 1)$ , and solving a simple linear equation:

$$\begin{cases} a_{R(i,j)} - a_{IR(i,j)} = \alpha_{i,j} \\ a_{R(i,j)} + a_{IR(i,j)} = 1 \end{cases}.$$

We can easily recover  $a_{R(i,j)} = \frac{1+\alpha_{i,j}}{2}$  and  $a_{IR(i,j)} = \frac{1-\alpha_{i,j}}{2}$ . As such, the *distinction* can be better captured while the *exclusiveness* is simultaneously secured. Specifically, we learn  $\alpha_{i,j}$  as

$$\alpha_{i,j} = \tanh(\mathbf{g} \left[ \mathbf{Z}_{R[i,:]}^{(k)} \oplus \mathbf{Z}_{IR[i,:]}^{(k)} \oplus \mathbf{Z}_{R[j,:]}^{(k)} \oplus \mathbf{Z}_{IR[j,:]}^{(k)} \right]^T), \quad (2)$$

where all the information is first concatenated and convoluted by  $\mathbf{g} \in \mathbb{R}^{1 \times 2d}$ , and then passed to the tangent activation function to produce a scalar value within  $(-1, 1)$ .

#### 4.2 Aggregation Layer

As the split network topologies disclose the partial relations among nodes in a latent space, they can be utilized to aggregate information

for learning different node aspects. Specifically, we leverage a simple low-pass filter with scaling parameters  $\{\epsilon_s | s \in \{R, IR\}\}$  for both task-relevant and irrelevant channels:

$$Z_s^{(k+1)} = \epsilon_s Z_s^{(0)} + (1 - \epsilon_s) D_s^{-\frac{1}{2}} A_s D_s^{-\frac{1}{2}} Z_s^{(k)}. \quad (3)$$

$D_s$  is the degree matrix associated with the adjacency matrix  $A_s$ . Derivation of Eq. (4.2) is detailed in our theoretical analysis. Importantly, by incorporating proximity information in different structural spaces, the task-relevant and irrelevant information can be better disentangled in  $Z_R^{(k+1)}$  and  $Z_{IR}^{(k+1)}$ , based on which the next ES-layer can make a more precise partition on the raw topology.

### 4.3 Irrelevant Consistency Regularization

Stacking ES-layer and aggregation layer iteratively lends itself to disentangling different features of nodes into the task-relevant and irrelevant representations, denoted by  $Z_R$  and  $Z_{IR}$  respectively. Reasonably,  $Z_R$  is granted for prediction, and the supervision signals through back-propagation gradually train  $Z_R$  to extract the most correlated features to the classification task. Meanwhile, we also expect  $Z_{IR}$  to capture the least relevant information for prediction, to further reduce the false information which may be mistakenly preserved in  $Z_R$ .

To attain this, we propose Irrelevant Consistency Regularization (ICR) that imposes a concrete meaning on  $Z_{IR}$ . The rationale is to enforce  $Z_{IR}$  towards the opposite direction of  $Z_R$ . Given any connected nodes  $v_i$  and  $v_j$ , we would expect  $Z_{IR[i,:]}$  and  $Z_{IR[j,:]}$  to be more similar if the larger disagreement between their labels is perceived. Measuring the label agreement between adjacent nodes should be the first step. There are several powerful techniques [13, 26] which have been developed. However, in this work, we find that using directly the joint probability from our model prediction works well, which does not require any trainable parameters.

In summary, our ICR can be formulated as:

$$\mathcal{L}_{ICR} = \sum_{(v_i, v_j) \in \mathcal{E}} (1 - \hat{y}_i^T \hat{y}_j) \|Z_{IR[i,:]} - Z_{IR[j,:]}\|_2, \quad (4)$$

where  $\hat{y}_i, \hat{y}_j \in \mathbb{R}^C$  are the predicted probability vector of nodes  $v_i, v_j$ , and  $\|\cdot\|_2$  denotes L2 distance. By doing so,  $Z_{IR}$  is encouraged to capture the task-irrelevant features with employing a local consistency among pairwise nodes of different classes.

### 4.4 Overall Algorithm

The overall pipeline of ES-GNN is detailed in Algorithm 1. Specifically, we adopt ReLU activation function in Eq. (4.1) to first map node features into two different channels, and then pass them with the adjacency matrix to an ES-layer for splitting the raw network topology into two exclusive parts. After that, these two partial network topologies are utilized to aggregate information in different structural spaces. It may be desirable to stack multiple ES-layers followed by aggregation steps to explore information beyond local neighborhood. Finally, a fully connected layer is appended to project the learned representations into class space  $\mathbb{R}^C$ . We integrate  $\mathcal{L}_{ICR}$  into the optimization process with the irrelevant consistency coefficient  $\lambda_{ICR}$  in Eq. (4.4), where  $\mathcal{L}_{pred} = -\frac{1}{|V_{trn}|} \sum_i^{V_{trn}} \mathbf{y}_i^T \log(\hat{\mathbf{y}}_i)$ . Additionally, to sufficiently take advantage of the possible supervision signals, we will substitute  $\hat{\mathbf{y}}_i$  in Eq. (4.3) with  $\mathbf{y}_i$  for nodes

---

#### Algorithm 1 Framework of ES-GNN

---

**Input:** Nodes Set:  $V$ , Edge Set:  $E$ , Adjacency Matrix:  $A \in \mathbb{R}^{|V| \times |V|}$ , Node Features:  $\{\mathbf{x}_i \in \mathbb{R}^f | \forall v_i \in V\}$ ,  $K$ : the number of layers.  $\epsilon_s$ : scaling hyper-parameters for channel  $s \in \{R, IR\}$ ,  $\mathbf{y}_i, \forall v_i \in V_{trn}$ : ground truth labels on the training set

**Param:**  $\mathbf{W}_R, \mathbf{W}_{IR} \in \mathbb{R}^{f \times d}$ ,  $\mathbf{W}_F \in \mathbb{R}^{d \times C}$ ,  $\mathbf{b}_F \in \mathbb{R}^C$ ,  $\mathbf{g}^{(k)} \in \mathbb{R}^{2d}$

1: // Project node features into two subspaces.

2: **for**  $s \in \{R, IR\}$  **do**

3:      $Z_s^{(0)} \leftarrow \sigma(\mathbf{W}_s^T \mathbf{X} + \mathbf{b}_s)$ .

4:      $Z_s^{(0)} \leftarrow \text{Dropout}(Z_s^{(0)})$  // Enabled only for training.

5: **end for**

6: // Stack Edge Splitting and Aggregation Layers.

7: **for** number layer  $k=0, 1, \dots, K-1$  **do**

8:     // Edge Splitting Layer.

9:     Initialize  $\mathbf{A}_R, \mathbf{A}_{IR} \in \mathbb{R}^{|V| \times |V|}$  with zeros.

10:    **for**  $\{v_i, v_j\} \in \mathcal{E}$  **do**

11:       $\alpha_{i,j} \leftarrow \tanh(\mathbf{g}^{(k)}^T [Z_{R[i,:]}^{(k)} \oplus Z_{IR[i,:]}^{(k)} \oplus Z_{R[j,:]}^{(k)} \oplus Z_{IR[j,:]}^{(k)}])$ .

12:       $\alpha_{i,j} \leftarrow \text{Dropout}(\alpha_{i,j})$  // Enabled only for training.

13:       $\mathbf{A}_{R,[i,j]} \leftarrow \frac{1+\alpha_{i,j}}{2}, \mathbf{A}_{IR,[i,j]} \leftarrow \frac{1-\alpha_{i,j}}{2}$ .

14:    **end for**

15:    // Aggregation Layer.

16:    **for**  $s \in \{R, IR\}$  **do**

17:       $Z_s^{(k+1)} \leftarrow \epsilon_s Z_s^{(0)} + (1 - \epsilon_s) D_s^{-\frac{1}{2}} A_s D_s^{-\frac{1}{2}} Z_s^{(k)}$ .

18:    **end for**

19: **end for**

20: // Prediction.

21:  $\hat{\mathbf{y}}_i = \text{softmax}(\mathbf{W}_F^T Z_{R[i,:]}^{(K)} + \mathbf{b}_F), \forall v_i \in V$ .

22: // Optimization with Irrelevant Consistency Regularization.

23:  $\mathcal{L}_{ICR} = \sum_{v_i, v_j \in E} (1 - \hat{\mathbf{y}}_i^T \hat{\mathbf{y}}_j) \|Z_{IR[i,:]} - Z_{IR[j,:]}\|_2$ .

24:  $\mathcal{L}_{pred} = -\frac{1}{|V_{trn}|} \sum_i^{V_{trn}} \mathbf{y}_i^T \log(\hat{\mathbf{y}}_i)$ .

25: Minimize  $\mathcal{L}_{pred} + \lambda_{ICR} \mathcal{L}_{ICR}$ .

---

provided in the training set  $V_{trn}$ .

$$\mathcal{L} = \mathcal{L}_{pred} + \lambda_{ICR} \mathcal{L}_{ICR}. \quad (5)$$

Finally, we also report in Table 1 the complexity of our proposed ES-GNN method in comparison with the state-of-the-arts which will be evaluated in the experimental section. Clearly, our method displays the same complexity to FAGCN [5] while being slightly overhead compared to GPR-GNN [7]. Here, we omit the related works, GEN [30] and WRGAT [27], as their complexity is obviously higher than others by involving reconstructing the whole graph.

## 5 THEORETICAL ANALYSIS

In this section, we investigate two important problems: (1) what limits the generalization power of the conventional GNNs on graphs beyond homophily, and (2) how the proposed ES-GNN breaks this limit and performs well on different types of networks. We will answer these questions by first analyzing the typical GNNs as graph signal denoising from a more generalized viewpoint. We then impose our Hypothesis 1 to derive ES-GNN.

**Table 1: Time complexity of the comparison models with one hidden layer as an example.**  $D_{max}$  represents the maximum node degree, and  $|\mathcal{E}_2|$  is the total number of neighbors in the second hop of nodes. Other symbols are earlier defined in the texts.

Methods	GCN	GAT	H2GCN	FAGCN	GPR-GNN	ES-GNN (Ours)
Complexity	$O((f+C) \mathcal{E} d)$	$O(((2+f) \mathcal{V} +(4+C) \mathcal{E} )d)$	$O(fd+ \mathcal{E} D_{max}+( \mathcal{E} + \mathcal{E}_2 )d)$	$O(((1+C+f) \mathcal{V} + \mathcal{E} )d)$	$O((f \mathcal{V} + \mathcal{E} C)d)$	$O(((1+C+f) \mathcal{V} + \mathcal{E} )d)$

## 5.1 Limited Generalization of Conventional GNNs

Recent studies [18, 38] have proved that most GNNs can be regarded as solving a graph signal denoising problem:

$$\arg \min_{\mathbf{Z}} \|\mathbf{Z} - \mathbf{X}\|_2^2 + \xi \cdot \text{tr}(\mathbf{Z}^T \mathbf{L} \mathbf{Z}), \quad (6)$$

where  $\mathbf{X} \in \mathbb{R}^{|V| \times f}$  is the input signal,  $\mathbf{L} \in \mathbb{R}^{|V| \times |V|}$  is the graph laplacian matrix, and  $\xi$  is a constant coefficient. The first term guides  $\mathbf{Z}$  to be close to  $\mathbf{X}$ , while the second term  $\text{tr}(\mathbf{Z}^T \mathbf{L} \mathbf{Z})$  is the laplacian regularization, which penalizes the similarity between pairwise nodes. One fundamental assumption made here is that similar nodes should have a higher tendency to connect each other (we refer it as the standard smoothness assumption on graphs). However, real-world networks typically exhibit diverse linking patterns of both assortativity and dissassortativity. Constraining smoothness on each node pair is prone to mistakenly preserve both of the task-relevant and irrelevant (or even misleading) information. Given that, we divide the original graph edges into two exclusive sets, and reformulate Eq. (5.1) as:

$$\arg \min_{\mathbf{Z}} \|\mathbf{Z} - \mathbf{X}\|_2^2 + \xi \sum_{(v_p, v_q) \in \mathcal{E}_R} \|\mathbf{Z}_p - \mathbf{Z}_q\|_2^2 + \xi \sum_{(v_m, v_n) \in \mathcal{E}_{IR}} \|\mathbf{Z}_m - \mathbf{Z}_n\|_2^2,$$

where  $\mathcal{E}_R$  and  $\mathcal{E}_{IR}$  respectively indicates the task-relevant and irrelevant node relations. Clearly, emphasizing the commonality between adjacent nodes in  $\mathcal{E}_R$  is beneficial for keeping task-correlated information only. However, smoothing node pairs in  $\mathcal{E}_{IR}$  conversely may bring in misleading information, thus possibly limiting the prediction performance of GNNs.

## 5.2 ES-GNN with Disentangled Smoothness

In this subsection, we show how ES-GNN breaks this limit by establishing its connection to a graph signal denoising problem generalized with a disentangled smoothness assumption.

Our Hypothesis 1 implicitly divides the original graph edge set  $\mathcal{E}$  into  $\mathcal{E}_R$  and  $\mathcal{E}_{IR}$ , on which the nodes obey the standard smoothness assumption with the task-relevant and irrelevant features, respectively. We further interpret this result as a disentangled smoothness assumption. As such, the traditional graph signal denoising problem can be generalized as:

$$\begin{aligned} \arg \min_{\mathbf{Z}_R, \mathbf{Z}_{IR}} & \|\mathbf{Z}_R - \mathbf{X}_R\|_2^2 + \|\mathbf{Z}_{IR} - \mathbf{X}_{IR}\|_2^2 \\ & + \xi \sum_{(v_i, v_j) \in \mathcal{E}} \left( a_{R(i,j)} \|\mathbf{Z}_{R[i,:]} - \mathbf{Z}_{R[j,:]}\|_2^2 + a_{IR(i,j)} \|\mathbf{Z}_{IR[i,:]} - \mathbf{Z}_{IR[j,:]}\|_2^2 \right) \end{aligned}$$

$$\text{s.t. } a_{R(i,j)} + a_{IR(i,j)} = 1, \text{ and } a_{R(i,j)}, a_{IR(i,j)} \in (0, 1),$$

where  $a_{R(i,j)}$  and  $a_{IR(i,j)}$  measure the degree to which the connection between nodes  $v_i$  and  $v_j$  are relevant and irrelevant to the learning task. Finally, we derive the following theorem:

**Theorem 1.** The proposed ES-GNN is equivalent to the solution to the generalized graph denoising problem with the disentangled smoothness assumption.

PROOF. Let  $\mathbf{X}_R$  and  $\mathbf{X}_{IR}$  be the results of mapping  $\mathbf{X}$  into different channels in Eq. (4.1), i.e.,  $\mathbf{X}_R = \mathbf{Z}_R^{(0)}$  and  $\mathbf{X}_{IR} = \mathbf{Z}_{IR}^{(0)}$ . Hypothesis 1 motivates us to define  $a_{R(i,j)}$  and  $a_{IR(i,j)}$  as the similarity between nodes in two aspects. Combining the above constraints, we can derive a linear system:

$$\begin{cases} a_{R(i,j)} + a_{IR(i,j)} = 1 \\ a_{R(i,j)} - a_{IR(i,j)} = \phi_{res}(\mathbf{Z}_{R[i,:]}, \mathbf{Z}_{R[j,:]}, \mathbf{Z}_{IR[j,:]}, \mathbf{Z}_{IR[i,:]}) \end{cases},$$

where  $\phi_{res}(\mathbf{Z}_{R[i,:]}, \mathbf{Z}_{R[j,:]}, \mathbf{Z}_{IR[j,:]}, \mathbf{Z}_{IR[i,:]})$  denotes the residual score between node similarities in task-relevant and task-irrelevant aspects. Solving the above equations, we can attain  $a_{R(i,j)}$  and  $a_{IR(i,j)}$  as the function of node features in two channels, i.e.,

$$a_{R(i,j)} = \frac{1 + \phi_{res}(\mathbf{Z}_{R[i,:]}, \mathbf{Z}_{R[j,:]}, \mathbf{Z}_{IR[i,:]}, \mathbf{Z}_{IR[j,:]})}{2} \quad (7)$$

$$a_{IR(i,j)} = \frac{1 - \phi_{res}(\mathbf{Z}_{R[i,:]}, \mathbf{Z}_{R[j,:]}, \mathbf{Z}_{IR[i,:]}, \mathbf{Z}_{IR[j,:]})}{2} \quad (8)$$

Here,  $\phi_{res}$  can be realized by our residual scoring mechanism in Eq. (4.1). Directly solving the generalized denoising problem with  $a_{R(i,j)}$  and  $a_{IR(i,j)}$  specified in Eq. (5.2) and Eq. (5.2) is not easy. The mixing variables and the introduced non-linear operator in  $\phi_{res}$  result in a complicated differentiation process. Instead, we can approach this problem by decoupling the learning of  $a_{R(i,j)}$ ,  $a_{IR(i,j)}$  from the optimization target, and employ an iterative stage learning, of which the convergent property can be guaranteed by deep learning techniques.

Suppose we have attained the task-relevant and irrelevant node features in the  $k^{th}$  round, i.e.,  $\mathbf{Z}_R^{(k)}$  and  $\mathbf{Z}_{IR}^{(k)}$ . In the first stage, we compute  $a_{R(i,j)}^{(k)}$  and  $a_{IR(i,j)}^{(k)}$  with  $\{\mathbf{Z}_{R[i,:]}^{(k)}, \mathbf{Z}_{R[j,:]}^{(k)}, \mathbf{Z}_{IR[i,:]}^{(k)}, \mathbf{Z}_{IR[j,:]}^{(k)}\}$  in Eq. (5.2) and Eq. (5.2), which in fact turns out to be our edge splitting layer in Section 4.1. In the second stage, injecting the computed values of  $a_{R(i,j)}^{(k)}$  and  $a_{IR(i,j)}^{(k)}$  relaxes the mixture of variables  $\mathbf{Z}_R$  and  $\mathbf{Z}_{IR}$  in the original optimization problem, which can then be disentangled into two independent targets (as all four penalized terms are positive):

$$\mathbf{Z}_R^{(k+1)} = \arg \min_{\mathbf{Z}_R^*} \mathcal{L}_R = \|\mathbf{Z}_R^* - \mathbf{Z}_R^{(0)}\|_2^2 + \xi \cdot \text{tr}(\mathbf{Z}_R^{*T} \mathbf{L}_R^{(k)} \mathbf{Z}_R^*) \quad (9)$$

$$\mathbf{Z}_{IR}^{(k+1)} = \arg \min_{\mathbf{Z}_{IR}^*} \mathcal{L}_{IR} = \|\mathbf{Z}_{IR}^* - \mathbf{Z}_{IR}^{(0)}\|_2^2 + \xi \cdot \text{tr}(\mathbf{Z}_{IR}^{*T} \mathbf{L}_{IR}^{(k)} \mathbf{Z}_{IR}^*), \quad (10)$$

where  $\mathbf{L}_R^{(k)} = \mathbf{D}_R^{(k)} - \mathbf{A}_R^{(k)}$ ,  $\mathbf{A}_{R[i,j]}^{(k)} = a_{R(i,j)}^{(k)}$ ,  $\mathbf{D}_R^{(k)}$  is the associated degree matrix, and a similar form is defined for  $\mathbf{L}_{IR}^{(k)}$  with  $a_{IR(i,j)}^{(k)}$ . Lemma 2, on the  $R$  channel as an example, further shows that our aggregation layer in Section 4.2 is approximately solving the two optimization problems in Eq. (5.2) and Eq. (5.2).

Therefore, stacking ES- and aggregation layers is equivalent to applying the above stage learning iteratively with  $\mathbf{Z}_{IR}^{(0)} = \mathbf{X}_R$  and  $\mathbf{Z}_R^{(0)} = \mathbf{X}_{IR}$ . Finally, we penalize the prediction loss  $\mathcal{L}_{pred}$  and the

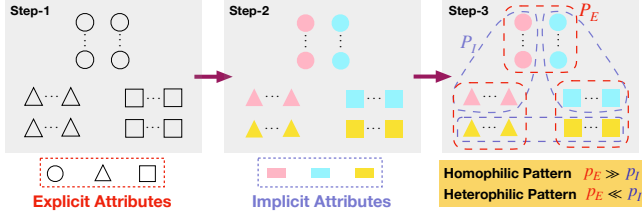


**Figure 2: Constructing synthetic graphs with arbitrary levels of homophily and heterophily. Shape and color of nodes illustrate the explicit and implicit attributes, respectively.**

irrelevant consistency loss  $\mathcal{L}_{ICR}$  based on  $Z_R^{(K)}$  and  $Z_{IR}^{(K)}$  in Eq. (4.4) with Adam [14] algorithm, which imposes concrete meanings on different channels and simultaneously ensures the convergence of our described stage learning.  $\square$

**Lemma 2.** When adopting the normalized laplacian matrix  $\mathbf{L}_R = \mathbf{I} - \mathbf{D}_R^{-\frac{1}{2}} \mathbf{A}_R \mathbf{D}_R^{-\frac{1}{2}}$ , the feature aggregation operator in Eq. (4.2) with channel  $s = R$  can be regarded as solving Eq. (5.2) using one-step gradient descent with  $\xi = \frac{1}{\epsilon_R} - 1$  and stepsize  $\beta = \frac{1}{2+2\xi}$ .

**PROOF.** We take one-step gradient descent with the stepsize  $\beta$  to solve the denoising problem in Eq. (5.2) as follows:

$$\begin{aligned} Z_R^{(k+1)} &= Z_R^{(k)} - \beta \cdot \frac{\partial \mathcal{L}_R}{\partial Z_R^*} \Big|_{Z_R^* = Z_R^{(k)}} \\ &= (1 - 2\beta - 2\beta\xi)Z_R^{(k)} + 2\beta Z_R^{(0)} + 2\beta\xi(\mathbf{D}_R^{-\frac{1}{2}} \mathbf{A}_R \mathbf{D}_R^{-\frac{1}{2}})Z_R^{(k)}. \end{aligned}$$

Setting  $\beta$  as  $\frac{1}{2+2\xi}$  gives us:

$$Z_R^{(k+1)} = \frac{1}{1+\xi}Z_R^{(0)} + \frac{\xi}{1+\xi}(\mathbf{D}_R^{-\frac{1}{2}} \mathbf{A}_R \mathbf{D}_R^{-\frac{1}{2}})Z_R^{(k)},$$

which is equivalent to Eq. (4.2) with  $\xi = \frac{1}{\epsilon_R} - 1$ .  $\square$

## 6 EXPERIMENTS

In this section, we empirically evaluate our ES-GNN for node classification using both synthetic and real-world datasets.

### 6.1 Datasets

**6.1.1 Synthetic Data.** To investigate the behavior of GNNs on graphs with arbitrary levels of homophily and heterophily, we construct synthetic graphs with our Hypothesis 1. The central idea is to define links among nodes under two conditions (i.e., task-relevant and irrelevant) independently, while only one of them is related to the classification task. We consider 1,200 nodes, 3 equal-size classes, and 500 features per node. First, we define both explicit and implicit attributes for nodes. The former depend on the label assignment, while the latter on the contrary model the class dependency. Specifically, we assign implicit attributes in a way such that nodes from different classes uniformly possess different kinds of pairs, as shown in Figure 2 (step-2). Notably, the attributes are combined into node features as the addition of different Gaussian random vectors. For example, the feature of a node with explicit attribute- $i$  (from class- $i$ ) and implicit attribute- $j$  are defined as the addition of two random vectors sampled from two different Gaussian distributions

**Table 2: Statistics of real-world datasets**

Datasets	# Nodes	# Edges	# Features	# Classes	$\mathcal{H}$	$\hat{\mathcal{H}}$
Chameleon	2,277	36,101	2,325	5	0.230	0.041
Squirrel	5,201	217,073	2,089	5	0.222	0.030
Actor	7,600	33,544	931	5	0.217	0.006
Twitch-DE	9,498	153,138	2,514	2	0.632	0.139
Cora	2,708	5,429	1,433	7	0.810	0.766
Citeseer	3,327	4,732	3,703	6	0.735	0.629
Pubmed	19,717	44,338	500	3	0.802	0.664
Polblogs	1,222	16,714	/	2	0.906	0.811

$\mathcal{N}(\mu_{E,i}, \sigma_{E,i})$  and  $\mathcal{N}(\mu_{I,j}, \sigma_{I,j})$ , respectively. After that, inspired by the Erdős-Rényi random graphs, we connect nodes with probability  $P_E$  if they are from the same class, with probability  $P_I$  if they share similar implicit attributes, and with probability  $q$  otherwise. We set  $q$  as  $1e-5$  to ensure the graph is connected, and use the widely adopted indexes  $\mathcal{H} = \frac{|\{(v_i, v_j) | (v_i, v_j) \in \mathcal{E}, y_i = y_j\}|}{|\mathcal{E}|}$  [7, 36, 37] to measure the homophily ratio of a graph. Intuitively, we anticipate heterophilic pattern when setting  $P_E \ll P_I$ , and strong homophily otherwise. Quantitatively, the relationship between the homophily ratio  $\mathcal{H}$  and parameters  $P_E, P_I$  can be derived with the simple combination in math and omitting the small value of  $q$ :

$$\mathcal{H}_{syn}(P_E, P_I) = \frac{3(n-3)}{3(n-3)+2n\frac{P_I}{P_E}}, \text{ where } n \text{ is the total number of nodes.}$$

Clearly, we have  $\mathcal{H}_{syn} \rightarrow 0$  while  $P_I \gg P_E$ , and  $\mathcal{H}_{syn} \rightarrow 1$  while  $P_I \ll P_E$ . Additional information is available in the supplement.

**6.1.2 Real-World Datasets.** We consider 8 benchmark datasets including both four heterophilic graphs, i.e., Chameleon, Squirrel[24], Actor [28], and Twitch-DE[24], as well as four homophilic graphs including Cora, Citeseer, Pubmed [25], and Polblogs [1]. The detailed statistics are provided in Table 2 where  $\hat{\mathcal{H}}$  is another homophily metric [17] considering class imbalance.

## 6.2 Experimental Setup

**6.2.1 Data Splitting.** For heterophilic graphs, following [7, 23, 37], we divides each dataset into 60%/20%/20% corresponding to training/validation/testing. For homophilic graphs, we adopt the popular sparse splitting [15, 29, 31], i.e., 20 nodes per class, 500 nodes, and 1,000 nodes to train, validate, and test models. For each dataset, 10 random splits are created for evaluation.

**6.2.2 Baselines.** We compare our ES-GNN with 9 baselines including the state-of-the-art GNNs: 1) MLP is a simple multi-perception layer; 2) GCN [15] adopts Chebyshev expansion to approximate the graph laplacian efficiently; 3) SGC [31] simplifies GCN [15] by removing non-linear mapping; 4) GAT [29] employs an attention mechanism to adaptively utilize neighborhood information; 5) GEN [30] estimates a new graph to fit GNNs' working mechanism; 6) WRGAT [27] transforms the raw graph into a multi-relational graph to attain an enhanced assortativity level; 7) H2GCN [37] takes advantages of the homophily information dominant in the higher-order neighborhood of nodes; 8) FAGCN [5] adaptively captures and utilizes both low- and high-frequency graph signals for prediction; 9) GPR-GNN [7] introduces learnable GPR weights between different hop neighborhoods, and develop a universal adaptability to different node-label patterns.

**Table 3: Node classification accuracies (%) over 100 runs (Bold: best) where Error Reduction gives the average improvement of ES-GNN upon the second place models (explicitly designed for heterophilic graphs).**

Models	Heterophilic Graphs				Homophilic Graphs			
	Squirrel	Chameleon	Twitch-DE	Actor	Cora	Citeseer	Pubmed	Polblogs
MLP	33.6 $\pm$ 1.3	47.4 $\pm$ 1.6	69.5 $\pm$ 1.2	38.1 $\pm$ 1.2	56.9 $\pm$ 1.7	56.6 $\pm$ 2.9	70.4 $\pm$ 2.3	81.8 $\pm$ 1.1
SGC [31]	50.7 $\pm$ 1.3	61.9 $\pm$ 2.6	73.9 $\pm$ 1.3	30.9 $\pm$ 0.6	79.1 $\pm$ 1.0	69.9 $\pm$ 2.0	76.6 $\pm$ 1.3	89.0 $\pm$ 1.5
GCN [15]	55.2 $\pm$ 1.5	67.6 $\pm$ 2.0	74.0 $\pm$ 1.2	31.2 $\pm$ 1.3	79.7 $\pm$ 1.2	69.5 $\pm$ 1.7	78.7 $\pm$ 1.6	89.4 $\pm$ 0.9
GAT [29]	54.8 $\pm$ 2.2	67.3 $\pm$ 2.2	73.7 $\pm$ 1.3	30.5 $\pm$ 1.2	82.0 $\pm$ 1.1	69.9 $\pm$ 1.7	78.6 $\pm$ 2.0	87.4 $\pm$ 1.1
GEN [30]	36.0 $\pm$ 4.0	57.6 $\pm$ 3.1	74.1 $\pm$ 1.4	37.3 $\pm$ 1.4	79.8 $\pm$ 1.3	69.7 $\pm$ 1.6	78.9 $\pm$ 1.7	89.6 $\pm$ 1.4
WRGAT [27]	39.6 $\pm$ 1.4	57.7 $\pm$ 1.6	70.0 $\pm$ 1.3	38.6 $\pm$ 1.1	71.7 $\pm$ 1.5	64.1 $\pm$ 1.9	73.3 $\pm$ 2.1	88.2 $\pm$ 1.2
H2GCN [37]	45.1 $\pm$ 1.9	62.9 $\pm$ 1.9	73.1 $\pm$ 1.5	38.4 $\pm$ 1.0	81.4 $\pm$ 1.4	68.7 $\pm$ 2.0	78.0 $\pm$ 2.0	89.0 $\pm$ 1.0
FAGCN [5]	50.4 $\pm$ 2.6	68.9 $\pm$ 1.8	74.1 $\pm$ 1.4	37.9 $\pm$ 1.0	82.6 $\pm$ 1.3	70.3 $\pm$ 1.6	80.0 $\pm$ 1.7	89.3 $\pm$ 1.1
GPR-GNN [7]	54.1 $\pm$ 1.6	69.6 $\pm$ 1.7	74.0 $\pm$ 1.6	38.0 $\pm$ 1.1	81.5 $\pm$ 1.5	69.6 $\pm$ 1.7	79.8 $\pm$ 1.3	89.5 $\pm$ 0.8
ES-GNN (ours)	<b>62.4<math>\pm</math>1.4</b>	<b>72.3<math>\pm</math>2.1</b>	<b>74.7<math>\pm</math>1.1</b>	<b>38.9<math>\pm</math>0.8</b>	<b>83.0<math>\pm</math>1.1</b>	<b>70.7<math>\pm</math>1.7</b>	<b>80.7<math>\pm</math>1.4</b>	<b>89.7<math>\pm</math>0.9</b>
Error Reduction	17.4%	9.0%	1.6%	0.9%	3.6%	2.2%	2.7%	0.6%

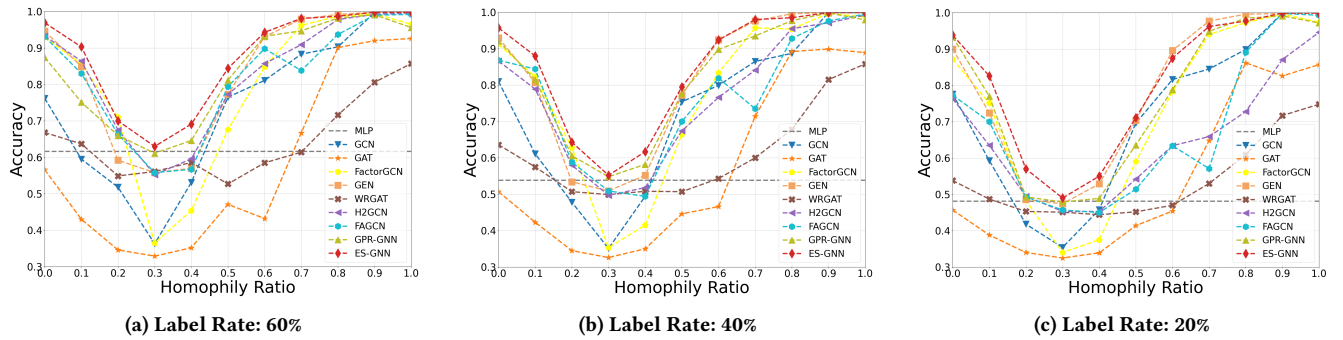


**Figure 3: Results of different models on synthetic graphs with varied homophily ratios.**

**6.2.3 Implementation Details.** For all the baselines and our model, we set  $d = 64$  as the number of hidden states for fair comparison, and tune the hyper-parameters on the validation split of each dataset using Optuna [2] for 200 trials. The searching space of hyper-parameters is specified in the supplementary material for reproducibility. With the best hyper-parameters, we train models in 1,000 epochs using the early-stopping strategy with a patience of 100 epochs. We then report the average performance in 10 runs on the test set for each random split.

### 6.3 Node Classification

**6.3.1 Results on Synthetic Graphs.** We examine the learning ability of various models on graphs across the homophily or heterophily spectrum. To more comprehensively evaluate our model, we consider three different label rates, i.e., 60%, 40%, and 20% nodes for training. From Figure 3, we have the following observations: 1) Looking through the overall trend, we obtain a “U” pattern on graphs from the lowest to the highest homophily ratios. That shows that GNNs’ prediction performance is not strictly correlated with the homophily level on graphs in a positive way. When it comes to the extreme heterophilic scenario, GNNs tend to alternate node features completely between different classes, thereby still making nodes distinguishable with respect to their labels. 2) Despite the

attention mechanism for adaptively utilizing relevant neighborhood information, GAT turns out to be the least robust method to arbitrary graphs. The entangled information in the mixed assortativity and disassortativity provides weak supervision signals for learning the attention weights. 3) The proposed ES-GNN consistently outperforms, or matches, others across different graphs with different homophily levels, especially in the hardest case with  $\mathcal{H} = 0.3$  where some baselines even perform worse than MLP. That is mainly because our ES-GNN is able to distinguish between task-relevant and irrelevant graph links, and disentangle the most correlated features for prediction.

**6.3.2 Results on Real-World Graphs.** Table 3 summarizes the node classification accuracies in 100 runs with multiple random splits on real-world data and different model initializations. In general, ES-GNN consistently performs better, or matches all the comparison methods. Specifically, it achieves significant performance gains, compared to the second place model, by 17.4% and 9.0% on the heterophilic graphs Squirrel and Chameleon, respectively. On Actor and Twitch-DE, ES-GNN wins by a margin of 1.6% and 0.9%, the state-of-the-arts, respectively. For graphs with strong homophily, ES-GNN maintains competitiveness and exhibits averagely 2.3% superiority upon the second place models. We will show our ES-GNN

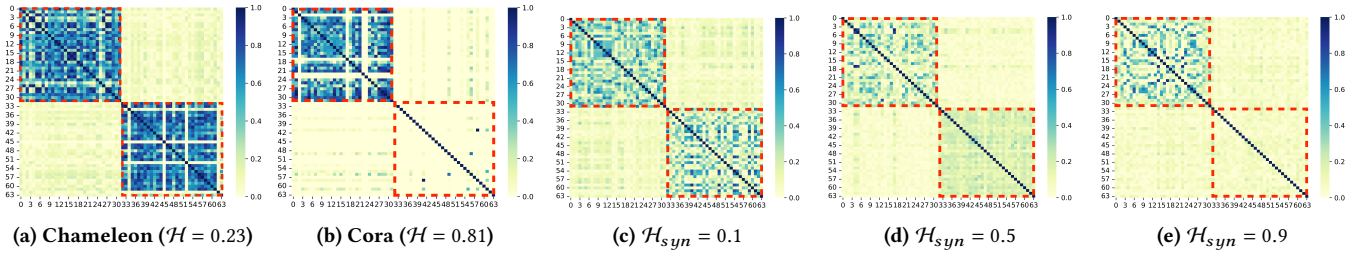


**Figure 4: Feature correlation analysis.** Two distinct patterns (task-relevant and task-irrelevant topologies) can be learned on Chameleon with  $\mathcal{H} = 0.23$ , while almost all information is retained in the task-relevant channel (0-31) on Cora with  $\mathcal{H} = 0.81$ . On synthetic graphs in (c), (d), and (e), block-wise pattern in the task-irrelevant channel (32-63) is gradually attenuated with the incremental homophily ratios across 0.1, 0.5, and 0.9. ES-GNN presents one general framework which can be adaptive for both heterophilic and homophilic graphs.

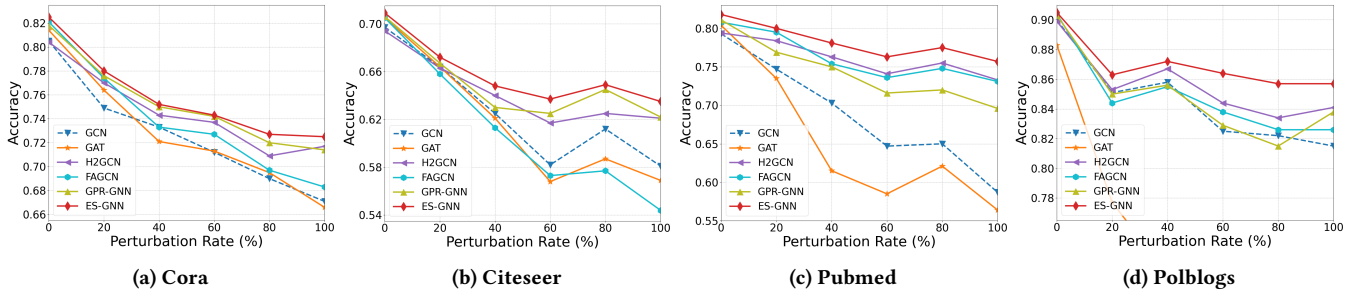


**Figure 5: Results of different models on perturbed homophilic graphs.**

could demonstrate remarkable robustness on homophilic graphs in case of perturbation or noisy links in Section 6.4.

#### 6.4 Robustness Analysis

By splitting the original graph edge set into task-relevant and task-irrelevant subsets, our proposed ES-GNN enjoys strong robustness particularly on homophilic graphs, since perturbed or noisy aspects of nodes could be purified from the task-relevant topology and disentangled in the task-irrelevant topology. To examine this, we randomly inject fake edges into graphs with perturbed rates from 0% to 100% with a step size of 20%. Adversarially perturbed examples are generated from graphs with strong homophily, such as Cora, Citeseer, Pubmed, and Polblogs. As shown in Figure 5, models considering graphs beyond homophily, i.e., H2GCN, FAGCN, GPR-GNN, and our model, consistently display a more robust behavior than GCN and GAT. That is mainly because fake edges may connect nodes across different labels, and consequently cause erroneous information sharing in the conventional methods.

On the other hand, our ES-GNN beats all the state-of-the-arts by an average margin of 2% to 3% on Citeseer, Pubmed, and Polblogs while displaying relatively the same results on Cora. We attribute this to the capability of our model in associating node connections with learning tasks. Take Pubmed dataset as an example. We investigate the learned task-relevant topologies and find that 81.0%, 73.0%, 82.1%, 83.0%, 82.6% fake links get removed on graphs under perturbation rates from 20% to 100%. This offers evidence supporting that the proposed ES-layer is able to distinguish between task-relevant

and irrelevant node connections. Therefore, despite a large number of false edge injections, the proximity information of nodes can still be reasonably mined in our model to predict their labels. Importantly, these empirical results also indicate that ES-GNN can still identify most of the task-irrelevant edges though no clear similarity or association between the connected nodes exists in the adversarial setting, which further relaxes our model from Hypothesis 1.

#### 6.5 Correlation Analysis

To better understand our proposed method, we investigate the disentangled features on Chameleon, Cora, and three synthetic graphs as typical examples in Figure 4. Clearly, on the strong heterophilic graph Chameleon, correlation analysis of learned latent features displays two clear block-wise patterns, each of which represents task-relevant or task-irrelevant aspect respectively. In contrast, on the citation network Cora, the node connections are in line with the classification task, since scientific papers mostly cite or are cited by others in the same research topic. Thus, most information will be retained in the task-relevant topology, while very minor information could be disentangled in the task-irrelevant topology (see Figure 4b). On the other hand, the results on synthetic graphs from Figure 4c to 4e display an attenuating trend on the second block-wise pattern with the incremental homophily ratios across 0.1, 0.5, and 0.9. This correlation analysis empirically verifies that our ES-GNN successfully disentangles the task-relevant and irrelevant features, and also demonstrates its universal adaptivity on different types of networks.

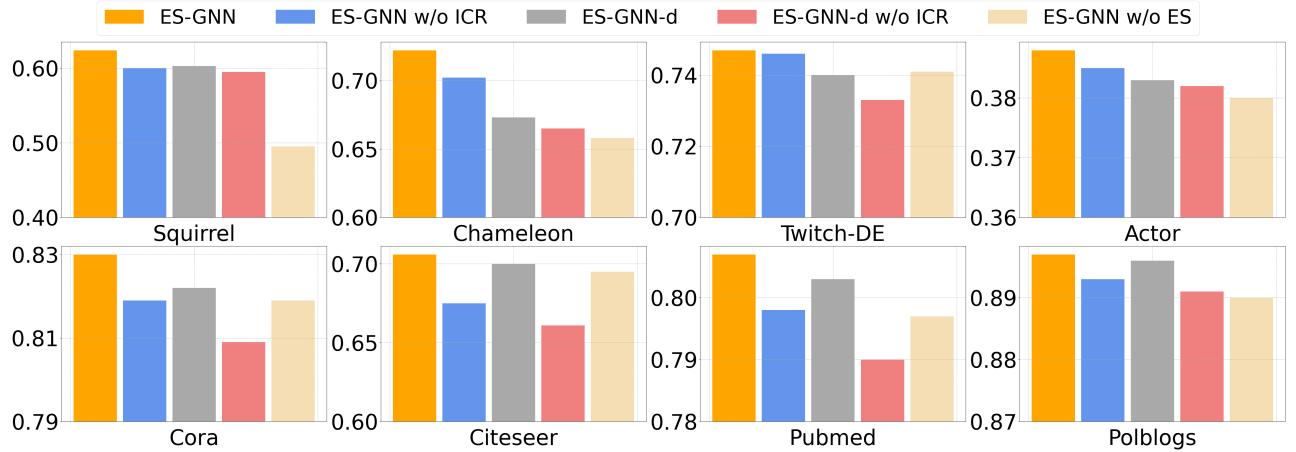


Figure 6: Ablation study of ES-GNN on eight datasets in node classification.

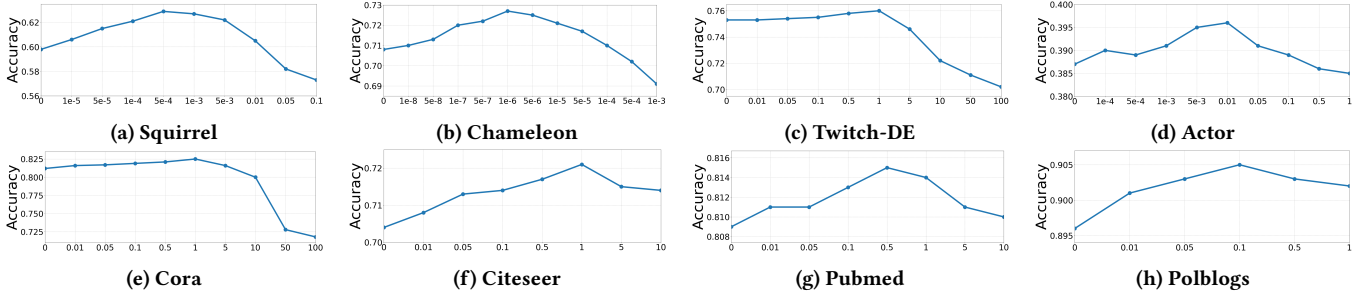


Figure 7: Sensitivity analysis of Coefficient  $\lambda_{ICR}$ .

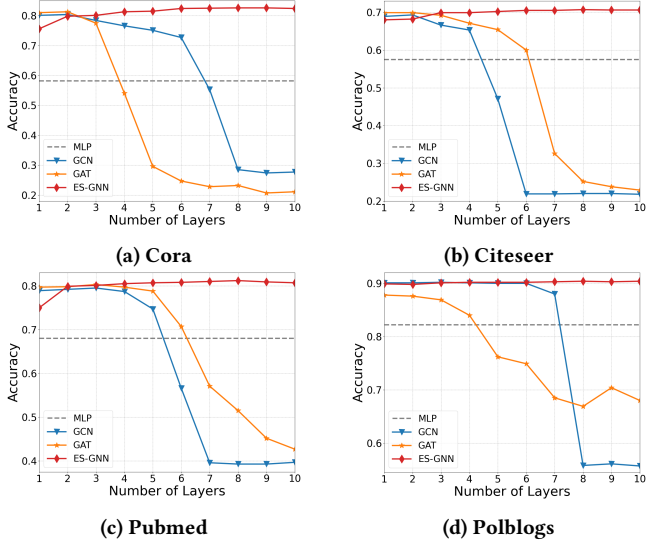


Figure 8: Classification accuracy vs. model depths.

## 6.6 Alleviating Over-smoothing Problem

In order to verify whether ES-GNN alleviates the over-smoothing problem, we compare it with GCN and GAT by varying the layer number in Figure 8. It can be observed that these two baselines attain their highest results when the number of layers reaches around two. As the layer goes deeper, the accuracies of both GCN and GAT gradually drop to a lower point. On the contrary, our ES-GNN presents a stable curve. In spite of starting from a relative lower point, the performance of ES-GNN keeps improving as the model depths increase, and eventually outperforms both GCN and GAT. The main reason is that, our ES-GNN can adaptively utilize proper graph edges in different layers to attain the task-optimal results. In other words, once an edge stops passing useful information or starts passing misleading messages, ES-GNN tends to identify it and remove it from learning the task-correlated representations, thereby having the ability of mitigating the over-smoothing problem.

## 6.7 Channel Analysis and Ablation Study

In this section, we compare ES-GNN with its variant ES-GNN-d which takes dual (both the task-relevant and irrelevant) channels for prediction, and perform an ablation study. Figure 6 provides comparison on eight real-world datasets. Here, we first specify some annotations including 1) “w/o ICR”: without regularization loss  $\mathcal{L}_{ICR}$ , and 2) “w/o ES”: without edge splitting (ES-) layer. Overall,

two conclusions can be drawn from Figure 6. First, ES-GNN is consistently better than ES-GNN-d, implying that the task-irrelevant channels indeed capture some false information where model performance downgrades even with the doubled feature dimensions. Second, removing either ICR or ES-layer from both ES-GNN and ES-GNN-d leads to a clear accuracy drop. That validates the effectiveness of our model design.

## 6.8 Sensitivity Analysis of Coefficient $\lambda_{ICR}$

We test the effect of the irrelevant consistency coefficient  $\lambda_{ICR}$ , and plot the learning performance of our model on eight real-world datasets in Figure 7 by varying  $\lambda_{ICR}$  with different values. For example, the classification accuracy on Squirrel in Figure 7a goes up first and then gradually drops. Promising results can be attained by choosing  $\lambda_{ICR}$  from  $[5e-5, 5e-3]$ . Similar trends can be also observed on the other datasets, where  $\lambda_{ICR}$  is relatively robust within a wide albeit distinct interval.

## 7 CONCLUSION

In this paper, we develop a novel graph learning framework which generalizes GNNs beyond homophily. We manage to cope with the mismatch between connected nodes in heterophilic settings and disentangle the original graph structure into two interpretable task-relevant and task-irrelevant topologies. Theoretical analysis illustrates our motivation and offers interpretations on the expressive power of ES-GNN on different types of networks. Extensive experiments over 8 benchmark and 1 synthetic datasets show that ES-GNN outperforms the other 10 recent competitive GNNs across both graphs with homophily and heterophily.

## REFERENCES

[1] Lada A Adamic and Natalie Glance. 2005. The Political Blogosphere and the 2004 US Election: Divided They Blog. In *Proceedings of the 3rd international workshop on Link discovery*. 36–43.

[2] Takuwa Akiba, Shotaro Sano, Toshihiko Yanase, Takeru Ohta, and Masanori Koyama. 2019. Optuna: A Next-generation Hyperparameter Optimization Framework. In *Proceedings of the 25th ACM SIGKDD international conference on knowledge discovery & data mining*. 2623–2631.

[3] Miltiadis Allamanis, Marc Brockschmidt, and Mahmoud Khademi. 2018. Learning to Represent Programs with Graphs. *ArXiv abs/1711.00740* (2018).

[4] Muhammet Balciar, Pierre Héroux, Benoit Gauzere, Pascal Vasseur, Sébastien Adam, and Paul Honeine. 2021. Breaking the Limits of Message Passing Graph Neural Networks. In *International Conference on Machine Learning*. PMLR, 599–608.

[5] Deyu Bo, Xiao Wang, Chuan Shi, and Huawei Shen. 2021. Beyond Low-frequency Information in Graph Convolutional Networks. In *AAAI*. AAAI Press.

[6] Tianwen Chen and Raymond Chi-Wing Wong. 2020. Handling Information Loss of Graph Neural Networks for Session-based Recommendation. In *Proceedings of the 26th ACM SIGKDD International Conference on Knowledge Discovery & Data Mining*. 1172–1180.

[7] Eli Chien, Jianhao Peng, Pan Li, and Olgica Milenkovic. 2021. Adaptive Universal Generalized PageRank Graph Neural Network. In *International Conference on Learning Representations*. <https://openreview.net/forum?id=n6j17fLxrP>

[8] Lukas Faber, Amin K. Moghaddam, and Roger Wattenhofer. 2021. When Comparing to Ground Truth is Wrong: On Evaluating GNN Explanation Methods. In *Proceedings of the 27th ACM SIGKDD Conference on Knowledge Discovery & Data Mining*. 332–341.

[9] Justin Gilmer, Samuel S Schoenholz, Patrick F Riley, Oriol Vinyals, and George E Dahl. 2017. Neural Message Passing for Quantum Chemistry. In *International Conference on Machine Learning*. PMLR, 1263–1272.

[10] Yifan Hou, Jian Zhang, James Cheng, Kaili Ma, Richard TB Ma, Hongzhi Chen, and Ming-Chang Yang. 2019. Measuring and Improving the Use of Graph Information in Graph Neural Networks. In *International Conference on Learning Representations (ICLR)*.

[11] Han Huang, Leilei Sun, Bowen Du, Chuanren Liu, Weifeng Lv, and Hui Xiong. 2021. Representation Learning on Knowledge Graphs for Node Importance Estimation. In *Proceedings of the 27th ACM SIGKDD Conference on Knowledge Discovery & Data Mining*. 646–655.

[12] Di Jin, Ziyang Liu, Weihao Li, Dongxiao He, and Weixiong Zhang. 2019. Graph Convolutional Networks Meet Markov Random Fields: Semi-Supervised Community Detection in Attribute Networks. In *Proceedings of the AAAI Conference on Artificial Intelligence*, Vol. 33. 152–159.

[13] Dongkwan Kim and Alice Oh. 2021. How to Find Your Friendly Neighborhood: Graph Attention Design with Self-Supervision. In *International Conference on Learning Representations*. <https://openreview.net/forum?id=W15KUNlqWty>

[14] Diederik P Kingma and Jimmy Ba. 2014. Adam: A Method for Stochastic Optimization. *arXiv preprint arXiv:1412.6980* (2014).

[15] Thomas N. Kipf and Max Welling. 2017. Semi-Supervised Classification with Graph Convolutional Networks. In *International Conference on Learning Representations (ICLR)*.

[16] Kwei-Herng Lai, Daochen Zha, Kaixiong Zhou, and Xia Hu. 2020. Policy-GNN: Aggregation Optimization for Graph Neural Networks. In *Proceedings of the 26th ACM SIGKDD International Conference on Knowledge Discovery & Data Mining (KDD)*. 461–471.

[17] Derek Lim, Xiuyu Li, Felix Hohne, and Ser-Nam Lim. 2021. New Benchmarks for Learning on Non-Homophilous Graphs. *arXiv preprint arXiv:2104.01404* (2021).

[18] Yao Ma, Xiaorui Liu, Tong Zhao, Yozhen Liu, Jiliang Tang, and Neil Shah. 2021. A Unified View on Graph Neural Networks as Graph Signal Denoising. In *Proceedings of the 30th ACM International Conference on Information & Knowledge Management*. 1202–1211.

[19] Miller McPherson, Lynn Smith-Lovin, and James M Cook. 2001. Birds of a Feather: Homophily in Social Networks. *Annual review of sociology* 27, 1 (2001), 415–444.

[20] Yimeng Min, Frederik Wenkel, and Guy Wolf. 2020. Scattering GGN: Overcoming Oversmoothness in Graph Convolutional Networks. *Advances in Neural Information Processing Systems* 33 (2020), 14498–14508.

[21] Hoang Nt and Takanori Maehara. 2019. Revisiting Graph Neural Networks: All We Have is Low-pass Filters. *arXiv preprint arXiv:1905.09550* (2019).

[22] Kenta Oono and Taiji Suzuki. 2020. Graph Neural Networks Exponentially Lose Expressive Power for Node Classification. In *International Conference on Learning Representations*. <https://openreview.net/forum?id=S1ldO2EFPr>

[23] Hongbin Pei, Bingzhen Wei, Kevin Chen-Chuan Chang, Yu Lei, and Bo Yang. 2020. Geom-GCN: Geometric Graph Convolutional Networks. *ArXiv abs/2002.05287* (2020).

[24] Benedek Rozemberczki, Carl Allen, and Rik Sarkar. 2021. Multi-scale Attributed Node Embedding. *Journal of Complex Networks* 9, 2 (2021), cnab014.

[25] P. Sen, Galileo Namata, M. Bilgic, L. Getoor, B. Gallagher, and Tina Eliassi-Rad. 2008. Collective Classification in Network Data. *AI Mag.* 29 (2008), 93–106.

[26] Otilia Stretcu, Krishnamurthy Viswanathan, Dana Movshovitz-Attias, Emmanouil Antonios Platanios, Sujith Ravi, and Andrew Tomkins. 2019. Graph Agreement Models for Semi-Supervised Learning. In *NeurIPS*.

[27] Susheel Suresh, Vinith Budde, Jennifer Neville, Pan Li, and Jianzhu Ma. 2021. Breaking the Limit of Graph Neural Networks by Improving the Assortativity of Graphs with Local Mixing Patterns. *arXiv preprint arXiv:2106.06586* (2021).

[28] Ji Tang, Jimeng Sun, Chi Wang, and Zi Yang. 2009. Social Influence Analysis in Large-scale Networks. In *Proceedings of the 15th ACM SIGKDD international conference on Knowledge discovery and data mining*. 807–816.

[29] Petar Veličković, Guillem Cucurull, Arantxa Casanova, Adriana Romero, Pietro Liò, and Yoshua Bengio. 2018. Graph Attention Networks. *International Conference on Learning Representations* (2018). <https://openreview.net/forum?id=rJXmpikCZ> accepted as poster.

[30] Ruijia Wang, Shuai Mou, Xiao Wang, Wanpeng Xiao, Qi Ju, Chuan Shi, and Xing Xie. 2021. Graph Structure Estimation Neural Networks. In *Proceedings of the Web Conference 2021*. 342–353.

[31] Felix Wu, Amauri Souza, Tianyi Zhang, Christopher Fifty, Tao Yu, and Kilian Weinberger. 2019. Simplifying Graph Convolutional Networks. In *International Conference on Machine Learning*. PMLR, 6861–6871.

[32] Keyulu Xu, Chengtao Li, Yonglong Tian, Tomohiro Sonobe, Ken-ichi Kawarabayashi, and Stefanie Jegelka. 2018. Representation Learning on Graphs with Jumping Knowledge Networks. In *International Conference on Machine Learning*. PMLR, 5453–5462.

[33] Yiding Yang, Zunlei Feng, Mingli Song, and Xinchao Wang. 2020. Factorizable Graph Convolutional Networks. *Advances in Neural Information Processing Systems* 33 (2020).

[34] Rex Ying, Ruining He, Kaifeng Chen, Pong Eksombatchai, William L Hamilton, and Jure Leskovec. 2018. Graph Convolutional Neural Networks for Web-Scale Recommender Systems. In *Proceedings of the 24th ACM SIGKDD International Conference on Knowledge Discovery & Data Mining*. 974–983.

[35] Ziwei Zhang, Peng Cui, and Wenwu Zhu. 2020. Deep Learning on Graphs: A Survey. *IEEE Transactions on Knowledge and Data Engineering* (2020).

[36] Jiong Zhu, Ryan A Rossi, Anup Rao, Tung Mai, Nedim Lipka, Nesreen K Ahmed, and Danai Koutra. 2021. Graph Neural Networks with Heterophily. In *Proceedings of the AAAI Conference on Artificial Intelligence*, Vol. 35. 11168–11176.

[37] Jiong Zhu, Yujun Yan, Lingxiao Zhao, Mark Heimann, Leman Akoglu, and Danai Koutra. 2020. Beyond Homophily in Graph Neural Networks: Current Limitations

and Effective Designs. *Advances in Neural Information Processing Systems* 33 (2020).

[38] Meiqi Zhu, Xiao Wang, Chuan Shi, Houye Ji, and Peng Cui. 2021. Interpreting and Unifying Graph Neural Networks with An Optimization Framework. In *Proceedings of the Web Conference 2021*. 1215–1226.

## A SUPPLEMENTARY MATERIAL

### A.1 Synthetic Datasets

In this section, we provide more details about our synthetic datasets. To control the average degree of generated graphs, we need quantify its relationship with the parameters  $P_E$  and  $P_I$ . With a simple knowledge on combinatorics and statistics, we can derive the average graph degree approximately as a function of both  $P_E$  and  $P_I$ ,  $\mathcal{T}(P_E, P_I) = \frac{3P_E+4P_I}{9}n - P_E$ , where  $n$  is the number of nodes. Therefore, given fixed parameters  $P_E^*$  and  $P_I^*$  making the expected homophily ratio  $\mathcal{H}(P_E, P_I)$ , we can simply multiply a scaling parameter  $\kappa$  to constrain the average graph degree within a proper range, i.e., average degree =  $\kappa \cdot \mathcal{T}(\hat{P}_E, \hat{P}_I)$ . Table 4 provides values of all the parameters we used for constructing synthetic graphs with an average degree around 20 and different homophily ratios. Additionally, for each synthetic graph, we consider three label rates, i.e., 60%, 40%, and 20% nodes for training, and the rest are equally divided for validation and testing.

**Table 4: Parameter setting for constructing synthetic graphs with different homophily ratios  $\mathcal{H}$ .**

$\mathcal{H}$	0.0	0.1	0.2	0.3	0.4	0.5	0.6	0.7	0.8	0.9	1.0
$P_E$	0.02	0.06	0.1	0.2	0.4	0.4	0.6	0.7	0.8	0.9	0.96
$P_I$	0.72	0.81	0.6	0.7	0.9	0.6	0.6	0.45	0.3	0.15	0.045
$\kappa$	0.1	0.084	0.1	0.075	0.05	0.062	0.05	0.05	0.05	0.05	0.051

### A.2 Hyper-Parameter Setting

We provide the searching space of our hyper-parameters for reproducibility: learning rate  $lr \sim [1e-2, 1e-1]$ , weight decay  $reg \sim [1e-6, 1e-3]$ , dropout  $p \sim \{0, 0.1, 0.2, 0.3, 0.4, 0.5, 0.6, 0.7, 0.8\}$ , the number of layers  $K \sim \{1, 2, 3, 4, 5, 6, 7, 8\}$ , scaling parameter  $\epsilon_R, \epsilon_{IR} \sim \{0.1, 0.2, 0.3, 0.4, 0.5, 0.6, 0.7, 0.8, 0.9, 1\}$ , and irrelevant consistency coefficient  $\sim \lambda_{ICR} \sim [0, 1]$  for Cora, Citeseer, Pubmed, and Twitch-DE,  $\sim [5e-7, 5e-6]$  for Chameleon,  $\sim [1e-4, 5e-3]$  for Squirrel, and  $\sim [5e-3, 5e-2]$  for Actor.

### A.3 Feature Correlation Analysis

Figure 9 provides more results on the correlation analysis between different feature channels on real-world graphs, where similar results and trends according to the main text can be found.

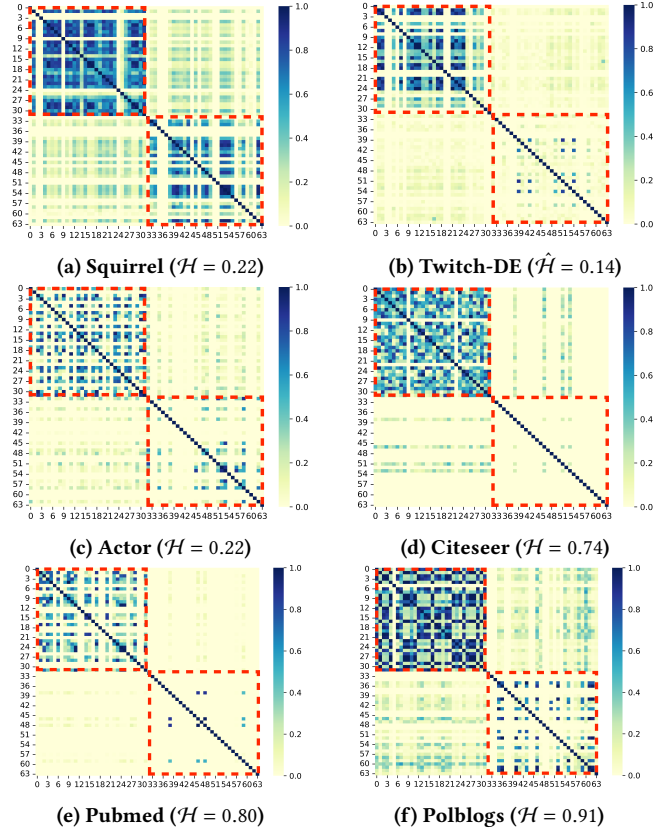


**Figure 9: Additional feature correlation analysis on real-world graphs.**